IEEJ Journal of Industry Applications
Vol.4 No.3 pp.187–195 DOI: 10.1541/ieejjia.4.187

Paper

Stability Analysis and Active Damping for *LLCL*-Filter-Based Grid-Connected Inverters

Min Huang[*a)] Non-member, Xiongfei Wang[*] Non-member
Poh Chiang Loh[*] Non-member, Frede Blaabjerg[*] Non-member
Weimin Wu[**] Non-member

(Manuscript received Aug. 9, 2014, revised Nov. 20, 2014)

A higher-order passive power filter (*LLCL* filter) for a grid-connected inverter is becoming attractive for the industrial applications owing to the possibility of reducing the cost of copper and the magnetic material. To avoid the well-known resonance problems of the *LLCL* filter, it is necessary to use either passive or active damping methods. In this study, the stability of the *LLCL*-filter-based grid-connected inverter is analyzed and a critical resonant frequency for the *LLCL* filter is identified when sampling and transport delays are considered. In the high-resonant-frequency region, active damping is not required; however, active damping is necessary in the low-resonant-frequency region. The basic *LLCL* resonance damping properties of different feedback states based on a notch filter concept are also studied. Then, an active damping method using capacitor current feedback for the *LLCL* filter is introduced. On the basis of this active damping method, a design procedure for the controller is given. Last, both simulation and experimental results are provided to validate the theoretical analysis of this study.

Keywords: *LLCL* filter, grid-connected converter, active damping, current control, resonant frequency, stability

1. Introduction

Recently, due to the energy crisis, Distributed Generation (DG) systems using clean renewable energy such as solar energy, wind energy, etc., have become an important issue in the technical research. The voltage Source Inverter (VSI) has increasingly been used to enable the integration of renewable power generations into the power grid [1]. Typically, a simple series inductor *L* is inserted between the voltage source inverter (VSI) and the grid to attenuate the high-frequency Pulse Width Modulation (PWM) harmonics to a desirable limit. But the high values of the *L* filter needs to be adopted to reduce the current harmonics around the switching frequency, which would lead to a poor dynamic response of the system and a high power loss. A low-pass passive power filter, the *LCL* filter, can achieve a high harmonic attenuation performance with less total inductance [2].

In order to further reduce the total inductance, the *LLCL* filter was proposed [3]. Compared with the *LCL* filter, the total inductance and volume of the *LLCL* filter can be reduced by 25%~40%. So, the *LLCL* filter for the grid-connected inverter is becoming attractive for industrial applications [4]. The applications of *LLCL* filter for a three-phase three-wire Shunt Active Power Filter (SAPF) [5] and a Large-Scale Wave Power Plant [6] have been analyzed.

As a high order filter, the *LLCL* filter has also a resonant problem. To suppress the possible resonances of an *LCL* filter or an *LLCL* filter, active damping [7]–[12] or passive damping [13]–[15] methods may be adopted. Passive damping is realized by adding additional components in the system but it causes a decrease of the overall system efficiency. For a stiff grid application, the passive damping strategy seems to be more attractive. In order to achieve a higher efficiency and flexibility, the active damping method might be preferred, although at the risk of higher cost of sensors and more control complexity. Normally, digital sampling and transport delays caused by controller and modulation, as well as discretization effects are taken into account. The delay will influence the stability of the system and when the resonant frequency varies, damping method is usually required in an *LCL* filter [9].

For *LLCL* filter, when the ratio of the resonant frequency to the control frequency is high the system can be stable without damping but the system robustness is not good if the resonant frequency is around the 1/6 of the control frequency. In this paper, all possible feedback states of currents and voltages of *LLCL* filter capacitors and inductors with different feedback transfer functions are considered. The results show how the various feedback signals need to be fed back based on notch concept in order to achieve resonance damping. Based on the available choices of feedback variables, active damping of the capacitor current control strategy is used for *LLCL* filter. The Proportional-Resonant (PR) controller is also used in this paper. PR can provide larger gain at the fundamental frequency to eliminate the steady state error compared with PI regulator [16].

First, the system and its stability are analyzed in Section 2. In Section 3, a more general analysis of different active

a) Correspondence to: Min Huang. E-mail: hmi@et.aau.dk
* Department of Energy Technology, Aalborg University 9220, Aalborg, Denmark
** Electrical Engineering, Shanghai Maritime University 201306, Shanghai, China

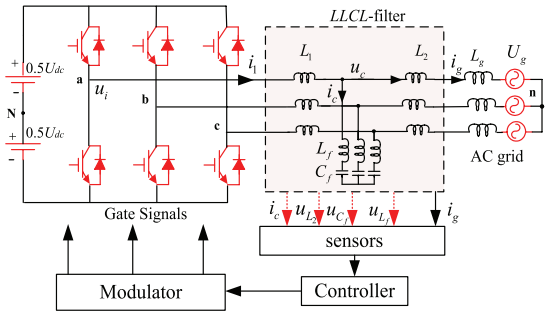

Fig. 1. General structure of three-phase grid-connected inverter with *LLCL* filter

Table 1. Test system parameters

DC link voltage U_{dc}	650 V	Grid frequency f_o	50 Hz
Grid phase voltage U_g	220 V	Sampling frequency f_d	10 kHz
Switching frequency f_s	10 kHz	Sampling period T_d	100 us

resonance damping solutions is carried out. The basic *LLCL* resonance damping properties of different feedback states are studied. In Section 4, design procedures of current controller and capacitor current feedback active damping are described. Last, simulated and experimental results are shown to verify the proposed design method.

2. Modeling and Stability of *LLCL*-Filter-Based Grid-Connected Inverter

2.1 Modeling of *LLCL*-Filter-Based Grid-Connected Inverter A three-phase voltage source converter connected to the grid via an *LLCL* filter is studied as shown in Fig. 1. U_{dc} is the dc input voltage of the inverter. The inverter output voltage and current are represented as u_i (phase voltage) and i_1, and the grid voltage and current are represented as u_g and i_g. i_c is the capacitor current, u_{Cf} is the output voltage of the capacitor, u_{Lf} is the output voltage of the resonant inductor, u_c is the voltage of L_f-C_f circuit and L_g is the grid impedance. The grid current feedback control will be discussed in this paper. The system parameters are given in Table 1.

Neglecting the influence of the grid impedance and the Equivalent Series Resistances (ESRs) of inductors and capacitors, the transfer function $i_g(s)/u_i(s)$ of the *LLCL* filter can be derived in (1).

$$G_{u_i \to i_g}(s) = \frac{L_f C_f s^2 + 1}{[L_1 L_2 C_f + (L_1 + L_2) L_f C_f] s^3 + (L_1 + L_2) s} \quad \cdots\cdots (1)$$

$$\omega_r = \frac{1}{\sqrt{\left(\frac{L_1 L_2}{L_1 + L_2} + L_f\right) C_f}} \quad \cdots\cdots (2)$$

As shown in (2), ω_r is the resonant frequency in radians per second), f_r is the resonant frequency in Hz. If the inductance of L_f is set to zero, then the transfer functions of the *LCL* filter can also be calculated. For voltage source converters the inverter-side current harmonics are dominated by the switching frequency. According to IEEE 519-1992 [17], harmonics higher than the 35th should be less than 0.3% of the rated fundamental current. Figure 2 shows bode plots of

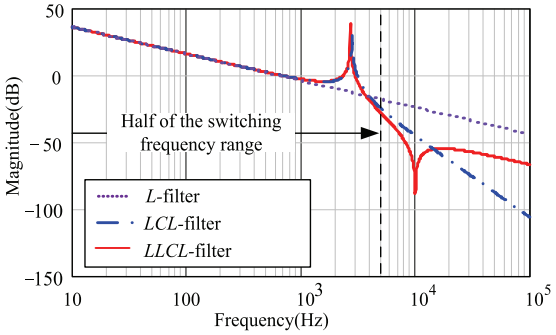

Fig. 2. Bode plots of transfer functions $i_g(s)/u_i(s)$ for different filters

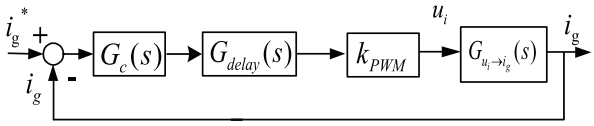

Fig. 3. Block diagram of grid current feedback control

transfer functions $i_g(s)/u_i(s)$ for different filters. For L filter, $L = 3.6$ mH. For *LCL* filter, $L_1 = 2.4$ mH, $L_2 = 1.2$ mH and $C_f = 4\,\mu$F. For *LLCL* filter, $L_1 = 2.4$ mH, $L_2 = 1.2$ mH, $L_f = 64\,\mu$H and $C_f = 4\,\mu$F. The characteristics of the three filters at the low frequencies are similar. The dominant harmonics of the grid-side current of the *LLCL* filter will be around the double of the switching frequency since the harmonics around the switching frequency are attenuated by the trap circuit L_f-C_f. That is the reason *LLCL* filter has smaller inductance or capacitance than *LCL* filter when they meet the same harmonic requirement of the grid-injected current [18].

According to (2), the resonant frequency of the *LLCL* filter can be higher than the resonant frequency of the *LCL* filter due to the smaller size. The ratio of the resonant frequency and the sampling frequency is related to the stability of *LCL* filter due to the delay [11]. It means that if an *LCL* filter with high resonant frequency is chosen the design of the active damping gets more difficult and a poorer robustness is obtained [19]–[22].

2.2 Stability of *LLCL*-Filter-Based Grid-Connected Inverter with Different Resonant Frequencies The control block diagram of a single loop controller of the *LLCL* filter based three-phase grid-connected inverter without any damping methods is shown in Fig. 3. T_d is the sampling period. The inverter can be modeled as a linear gain k_{PWM}, expressed as $k_{PWM} = 0.5U_{dc}$. $G_c(s)$ is a PR controller as shown in (3), where k_p and k_i are representing its proportional gain and the integral gain of the fundamental resonant frequency respectively. $G_{delay}(s)$ is the delay part in series with the forward path. In the s-domain one sample period delay $e^{-T_d s}$ is included due to computation in a real application. When the PWM reference is held on and compared to the triangular carrier to generate the duty cycle, a Zero-Order-Hold (ZOH) is in series of the open loop and discretization of the system introduces delay, as shown in (4). A PWM delay of half sampling period is introduced. Hence, the total delay in the continuous form is shown in (5).

$$G_c(s) = k_p + \frac{k_i s}{s^2 + (\omega_0)^2} \quad \cdots\cdots (3)$$

Table 2. *LLCL*-filter parameters and resonant frequency of three cases under study

Case I	Case II	Case III
L_1=2.4 mH	L_1=2.5 mH	L_1=3 mH
L_2=1.2 mH	L_2=2 mH	L_2=2.4 mH
C_f= 2 μF	C_f= 8 μF	C_f= 8 μF
L_f= 128 μH	L_f= 32 μH	L_f= 32 μH
f_r=3.69 kHz	f_r=1.67 kHz	f_r=1.52 kHz
f_r/f_d=0.369	f_r/f_d=0.167	f_r/f_d=0.153

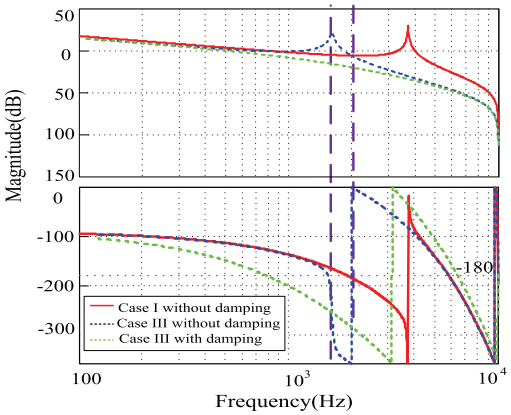

Fig. 4. Bode plot of the forward path transfer function for the grid current feedback control

$$H_o(s) = \frac{(1 - e^{-T_d s})}{s} \cdots\cdots (4)$$

$$G_{delay}(s) = e^{-1.5T_d s} \cdots\cdots (5)$$

$G(s)$ is the open transfer function of the grid current feedback control considering the total delay, which can be expressed as:

$$G(s) = G_{delay}(s) k_{PWM} G_c(s) G_{u_i \to i_g}(s) \cdots\cdots (6)$$

Table 2 shows three different cases with different resonant frequencies. Figure 4 shows the bode plot of the forward path transfer function for the grid current feedback control. It can be seen from Fig. 4 that the *LLCL* filter resonance has no influence on system stability when the resonant frequency is high (Case I), because the phase is already well below −180° before the re sonant frequency due to the sampling and transport delay. When the resonant frequency is low (Case III), the phase curve passes through −180° at the resonant frequency and the system is not stable without damping. When active damping is added in Case III, the resonance is damped and the system can be stable.

This analysis identifies that there is also a critical frequency for *LLCL* filter, and above it, active damping can be avoided by adjusting the controller gain.

$G_c(s)$ can be regarded as k_p at crossover frequency. When $\angle G_o(j\omega_k) = -\pi$, the phase of the single open loop is shown in (7). The root of the function can be calculated as $\omega_k = \pi/(3T_d)$. If a phase angle is already below −180° at this resonant frequency, the system can be stable. It can also be deduced that the critical frequency $f_k = f_d/6$.

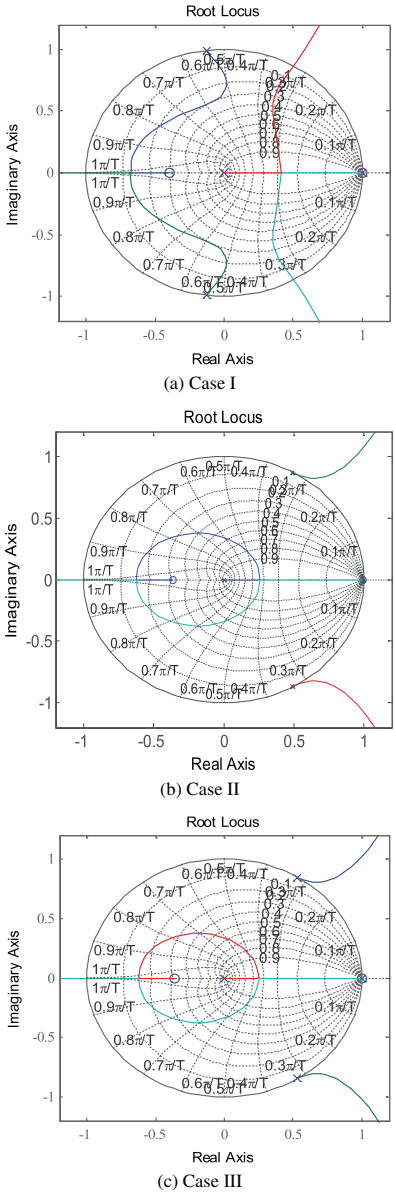

Fig. 5. Root loci of grid current feedback (without damping) of different cases specified in Table 2

$$\begin{aligned}\angle G(j\omega_k) &= \angle \left\{ \frac{e^{-j\omega_k T_d} \cdot \frac{1-e^{-j\omega_k T_d}}{j\omega_k}}{\frac{1-L_f C_f {\omega_k}^2}{j[(L_1+L_2)\omega_k - (L_1 L_2 C_f + (L_1+L_2) L_f C_f)\omega_k^3]}} \right\} \\ &= -\pi \cdots\cdots (7)\end{aligned}$$

Hence, a single loop is sufficient to be stable when the resonant frequency is above the critical frequency and active damping is necessary when the resonant frequency is below the critical frequency. As shown in Table 1, f_d is 10 kHz. Figure 5 shows the closed loop root loci of the three cases in Table 2 for the single loop grid current feedback in z-domain. A Zero-Order-Hold (ZOH) transform is applied on the transfer function $i_g(s)/u_i(s)$ of the *LLCL* filter. Figure 5(a) depicts the case when the resonant frequency of the *LLCL* filter is above the critical frequency. The poles initially track inside the unit circle. Figure 5(b) shows the case when the resonant frequency of the *LLCL* filter is at the critical frequency

and the system is on the edge to be unstable. When the resonant frequency is less than the critical frequency the system will always be unstable regardless of what the proportional gain is without damping, as shown in Fig. 5(c). In this case, a damping method is necessary to be used.

3. Active Damping with Different Feedback States

3.1 Notch Filter Concept Active damping methods can be classified into two main classes: multi-loop and filter-based active damping [7]. Traditionally, a notch filter is directly added in the current loop to compensate the resonant peak of the *LCL* filter. In order to provide a good damping the frequency of the Notch filter has to be tuned at the resonance frequency of the *LCL* filter. Notch filter concept can also be implemented by multi-loop control. The control structure of the inner current loop with a notch filter concept [22] is shown in Fig. 6.

$$B(s) = \frac{k_{PWM}}{1 + k_{PWM}K(s)N(s)} = \frac{s^2 + {\omega_r}^2}{s^2 + 2\zeta_2\omega_r s + {\omega_r}^2} \quad \cdots\cdots\cdots\cdots\cdots\cdots (8)$$

In order to eliminate the resonant peak at the frequency ω_r, the notch $B(s)$ should have a negative peak in ω_r, so it can be expressed as (8). There are different variables which can be chosen as the control object for *LLCL* filter. $K(s)$ is the feedback coefficient. Table 3 shows the transfer functions of different variables feedback. The structure of $N(s)$ depends on the feedback variables including the filter capacitor voltage u_{cf}, filter capacitor current i_c, filter resonant inductor voltage in grid side u_{L2}, inductor voltage in resonant circuit u_{Lf}. It can be seen from Table 3, the feedback function of the grid side inductor voltage is a little complex. The sensor location depends on the application situations. For different ratios between the resonant frequency and the control frequency, the selected approaches behave differently [10].

3.2 Filter Capacitor Current Feedback For the *LCL* filter, the capacitor current feedback and capacitor voltage feedback are often used [10]. When the capacitor current feedback is sensed, $K(s)$ can easily be configured as a proportional coefficient, which is isolated with the system

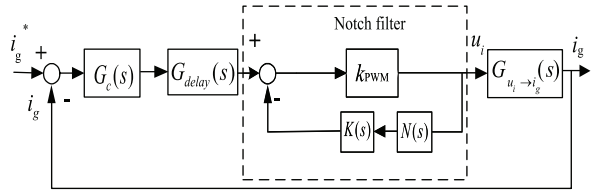

Fig. 6. Active damping based on a notch filter concept

parameters. $N(s)$ can be expressed as:

$$N(s) = G_{u_i \to i_c}(s) = \frac{{\omega^2}_r L_2 C_f s}{(s^2 + {\omega^2}_r)(L_1 + L_2)} \cdots\cdots\cdots\cdots (9)$$

Then the open loop transfer function of the capacitor current feedback control from i_g to ${i_g}^*$ is shown in (10).

The capacitor current feedback can dampen the resonant peak and make the system stable.

$$G'(s)_{|open} = \frac{k_{PWM}{\omega^2}_r(L_f C_f s^2 + 1)G_c(s)G_{delay}(s)}{(s^2 + {\omega^2}_r)(L_1 + L_2) + K_{i_c}G_{delay}(s)k_{PWM}L_2 s{\omega^2}_r} \frac{1}{s} \cdots\cdots\cdots\cdots\cdots (10)$$

3.3 Filter Capacitor Voltage Feedback When the capacitor voltage is sensed, a derivative filter capacitor voltage feedback can be used for the resonance damping. Some papers have illustrated this method for an *LCL* filter. As shown in Table 3, a differential feedback is necessary but it may cause noise problems in the control, because it will amplify high-frequency signals.

3.4 Filter Resonant Inductor Voltage Feedback When the resonant inductor voltage is sensed, the integral feedback can be expected to keep the system stable. Normally, the filter capacitor current or voltage is sensed for the *LCL* filter. This is a new active damping method for *LLCL* filter which can reduce the cost of sensors [23]. The feedback coefficient is integral and the structure of $N(s)$ is the transfer function from u_i to u_{Lf}.

The next section will only analyze the design of capacitor current feedback as an active damping method, as this is the most promising method.

4. Design of Current Regulator and Capacitor Current Feedback Coefficient

4.1 PR Controller Gain Design The maximum possible controller gains for the system can now be analytically determined using the concepts developed in (24)–(26). The proportional gain is then set to achieve unity gain at the desired crossover frequency f_c/ω_c. The choice of k_p can be decided by the system bandwidth satisfying the desired phase margin Φ_m [9]. For a single loop control, the phase angle at the crossover frequency can be described in (11). As shown in Fig. 2, the *LLCL* filter is approximate to an *L* filter in the low frequency. In addition, the cross-over frequency ω_c can be determined.

$$\omega_c = \frac{\pi/2 - \Phi_m}{3T_d/2} \cdots\cdots\cdots\cdots\cdots\cdots\cdots\cdots\cdots\cdots (11)$$

The system open-loop gain achieves unity at ω_c. Then the maximum gain can be calculated as:

Table 3. Transfer functions of different variables as feedback

Variable	u_{C_f}	i_c	u_{L_f}	u_{L_2}
$N(s)$	$\frac{{\omega^2}_r L_2}{(s^2+{\omega^2}_r)(L_1+L_2)}$	$\frac{{\omega^2}_r L_2 C_f s}{(s^2+{\omega^2}_r)(L_1+L_2)}$	$\frac{{\omega^2}_r L_2 C_f s^2}{(s^2+{\omega^2}_r)(L_1+L_2)}$	$\frac{{\omega^2}_r L_2 (L_f C_f s^2+1)}{(s^2+{\omega^2}_r)(L_1+L_2)}$
$K(s)$	$sK_{u_{C_f}}$	K_{i_c}	$K_{u_{L_f}} \big/ s$	$K_{u_{L2}} \frac{C_f s}{L_f C_f s^2+1}$

$$|G(j\omega_c)| \approx \left| \frac{k_p\sqrt{(\omega_c\tau)^2+1}}{\omega_c\tau} \right| \left| \frac{1-e^{-j\omega_c T_d}}{j\omega_c} \right| \left| \frac{k_{PWM}}{j(L_1+L_2)\omega_c} \right| \quad \cdots\cdots (12)$$

$$k_p \approx \frac{\omega_c(L_1+L_2)}{k_{PWM}} \quad \cdots\cdots (13)$$

4.2 Capacitor Current Feedback Coefficient Gain

The denominator of the closed loop transfer function of the *LLCL* filter is shown in (14) based on (10). The minimum value of K_{ic} can be found from (13) using the limiting ratio of the proportional gain k_p to dampen as shown in (14). According to the Routh's Stability Criterion, the range of K_{ic} can be obtained to be like given in (15).

$$D(s) = [L_1L_2C_f + (L_1+L_2)L_fC_f]s^4 + K_{i_c}k_{PWM}L_fL_2C_fs^3 + (L_1+L_2)s^2 + k_pk_{PWM}s + k_pk_ik_{PWM} \quad \cdots\cdots (14)$$

$$K_{i_c} \geq \frac{k_p}{(L_1+L_2)L_2}[L_1L_2 + (L_1+L_2)L_f] \quad \cdots\cdots (15)$$

$$K_{i_c} = 10^{GM_1/20}\frac{2\pi f_cL_1}{k_{PWM}} \quad \cdots\cdots (16)$$

$$K_{i_c} = 10^{GM_2/20}\left(\frac{6f_r}{f_d}\right)^2\frac{2\pi f_cL_1}{k_{PWM}} + \frac{2\pi f_cL_1}{k_{PWM}}\frac{(f_d/6)^2-(f_r)^2}{f_d/6} \quad \cdots\cdots (17)$$

GM_1 and GM_2 are defined by the gain margins of (10) at f_r and $f_d/6$ respectively [9]. Then the limitation of K_{ic} can be obtained from (16) and (17). $GM_1 > 0$ means the gain is lower than 0 dB at the corresponding frequency. When $f_r < f_d/6$, $GM_1 > 0$. When $f_r > f_d/6$, $GM_1 < 0$ and $GM_2 > 0$ to make sure the magnitude of the loop gain at $f_d/6$ must be lower than 0 dB and at f_r must be larger than 0 dB. (17) is the lower limitation and (16) is the upper limitation. K_{ic} should satisfy this region.

4.3 Design Example

Taken Case III as an example, the basic design procedures can be addressed as:

1) Determine the specifications of the loop gain. According to Case III, the resonant frequency is smaller than $f_d/6$, so GM_1 should be larger than 0. The desired phase margin Φ_m should be larger than 40° in order to get a good dynamic response and stability margin.
2) Obtain the value of k_p and f_c to satisfy all the requirements according to (11), (13) and (14), f_c = 1 kHz is chosen to obtain fast dynamic response. Then k_p is calculated as 0.06 according to (13).
3) Figure 7 shows the closed loop root locus branch of the system with the capacitor current coefficient increasing when k_p is set to 0.06. There is a stable range of K_{ic} which can be obtained as shown in Fig. 7. The calculated gain should follow the region. For Case III, the limitation region is from 0.024–0.032.
4) Taking f_c = 1 kHz and the calculated feedback gain in (15), (16) and (17) to check whether they satisfy the function and GM_1 is larger than 0.

5. Simulation and Experimental Results

5.1 Simulation Results

In order to illustrate the stability and verify the active damping method of the *LLCL* filter based grid-connected inverter, a three-phase inverter with 6 kW rated power is simulated using PLECS Blockset and MATLAB. This paper uses PR controller and SPWM modulation. The detailed system parameters are listed in Table 1.

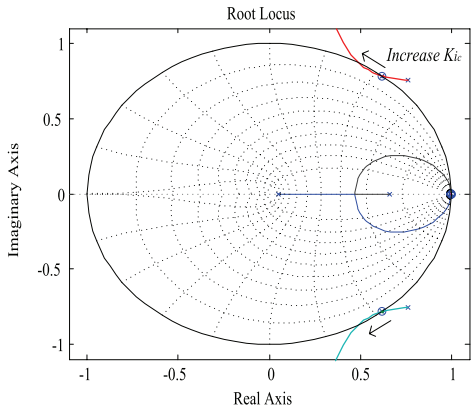

Fig. 7. Root loci of the system with K_{ic} increasing

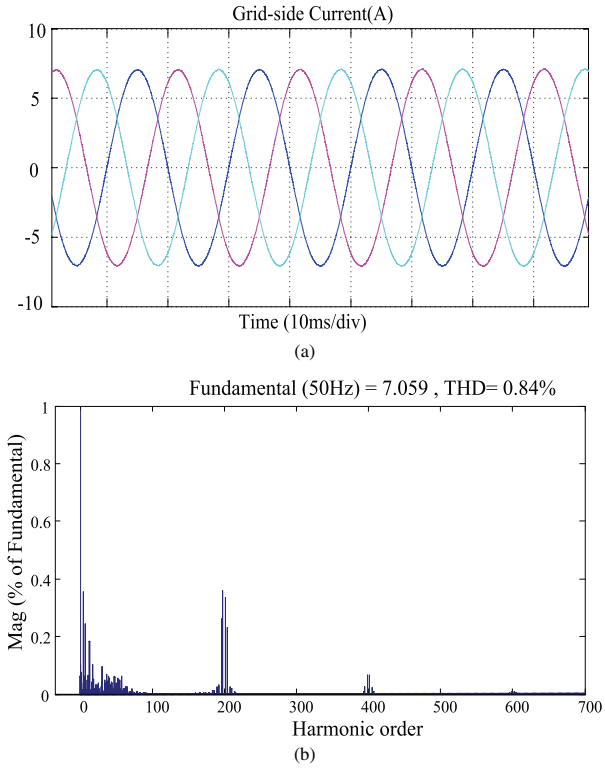

Fig. 8. Grid-side currents of *LCL* filter based inverter (a) Current waveforms and (b) The current spectrum

As discussed above, the *LLCL* filter can get the same harmonic attenuation as the *LCL* filter with a smaller inductance or capacitor which means *LLCL* filter has some superiority. A comparison is done by the simulations. Fig. 8 and Fig. 9 show the grid-side currents of *LCL* filter based inverter and *LLCL* filter based inverter respectively. For the *LCL* filter, L_1 = 2.4 mH, L_2 = 1.2 mH and C_f = 4 μF; For *LLCL* filter, L_1 = 2.4 mH, L_2 = 1.2 mH, L_f = 64 μH and C_f = 4 μF. The grid-current THD of *LCL* filter based inverter is 0.84% and harmonics around switching frequency are higher than 0.3% of the fundamental current. The grid-current THD of *LLCL* filter based inverter is 0.61% and dominant harmonics are around the double of the switching frequency. It shows the *LLCL* filter has better harmonics attenuation compared to the *LCL* filter.

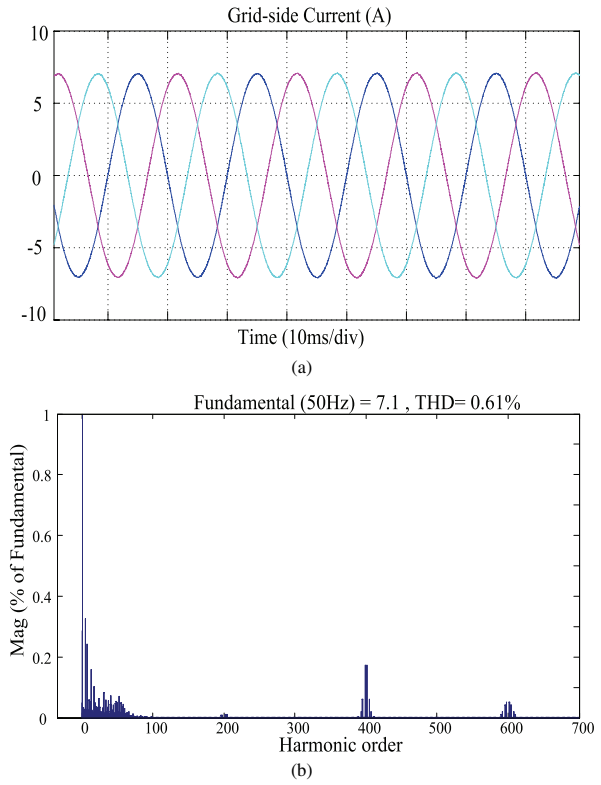

Fig. 9. Grid-side currents of the *LLCL* filter based inverter (a) Current waveforms and (b) The current spectrum

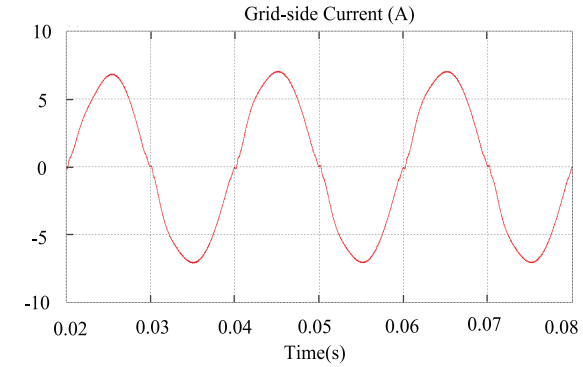

Fig. 10. Grid-side current waveform of Case I (f_{res} = 3.69 kHz)

Then, in order to investigate the stability of the system without damping in different resonant frequencies, the *LLCL* filter is analyzed into three cases as shown in Table 2, with different parameters: one with a high resonant frequency, one with a critical resonant frequency and the other with a low resonant frequency. According to (11), the controller gain is $k_p = 0.06$ and $k_i = 20$.

(1) Case I: high frequency f_{res} =3.69 kHz

In the Case I, the resonant frequency is high (3.69 kHz) and the crossover frequency is set to 1 kHz in order to get a fast response and to meet a phase margin limitation. It can be seen from Fig. 10 the system is stable.

(2) Case II: critical frequency f_{res} = 1.67 kHz

As it mentioned before, there is a critical frequency for the *LLCL* filter. It is calculated as $f_d/6$ based on the function (7). It can be seen from Fig. 11, the system is almost unstable at the critical frequency. When the grid impedance i_g is increased, the resonant frequency will be deduced more.

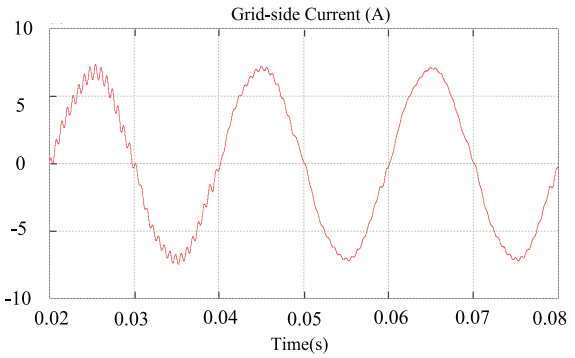

Fig. 11. Grid-side current waveform of Case II (f_{res} = 1.67 kHz)

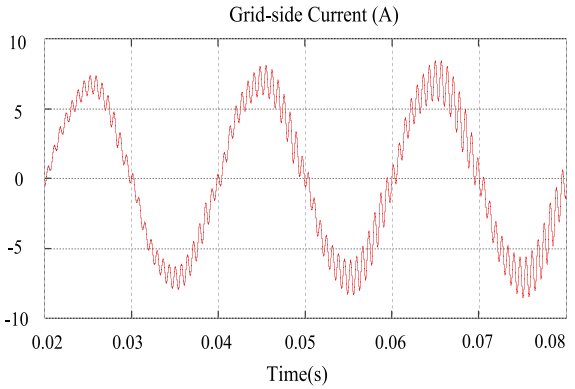

Fig. 12. Grid-side current waveform of Case II when $L_2 + L_g$ = 2.4 mH (f_{res} = 1.60 kHz)

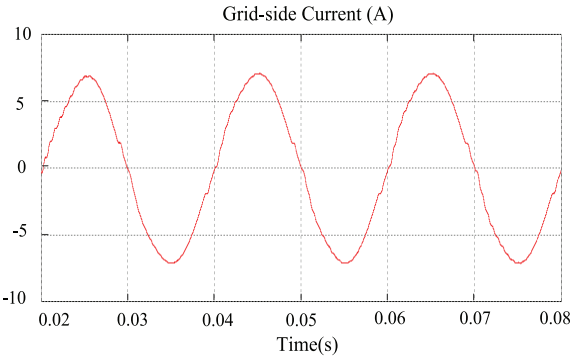

Fig. 13. Grid-side current waveform of Case II when $L_2 + L_g$ = 1.2 mH (f_{res} = 1.95 kHz)

As shown in Fig. 12, when the grid impedance L_g is set to 0.4 mH, the resonant frequency is reduced to 1.6 kHz, which is under the critical frequency and the system is unstable.

As shown in Fig. 13, when the grid-side inductance L_2 is changed to 1.2 mH, the resonant frequency is increased to 1.95 kHz and the system is changed from critical state to stable state.

(3) Case III: Low frequency f_{res} = 1.52 kHz

In Case III, the resonant frequency is low (1.52 kHz). It can be seen from Fig. 14 that the system is unstable without damping.

So, when designing the parameters it is better to make the resonant frequency higher in order to get a better stability and robustness. When the resonant frequency is lower or nearby the critical frequency, the active damping method is necessary to be used. In this paper, take Case III as an example,

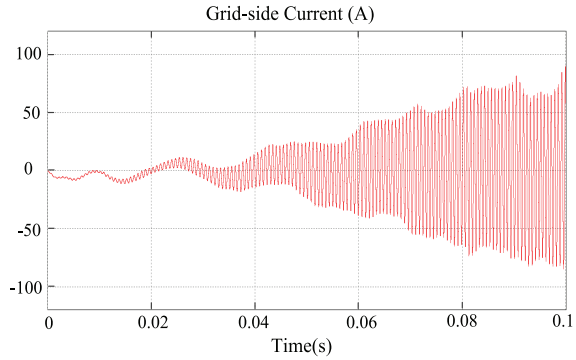

Fig. 14. Grid-side current waveform of Case III (f_{res} = 152 kHz)

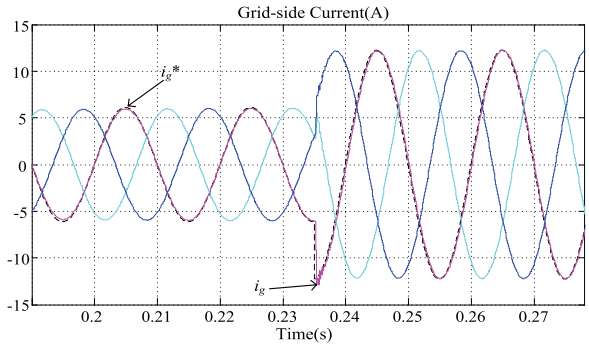

Fig. 15. Grid-side current waveforms of Case I (high resonant frequency) without active damping

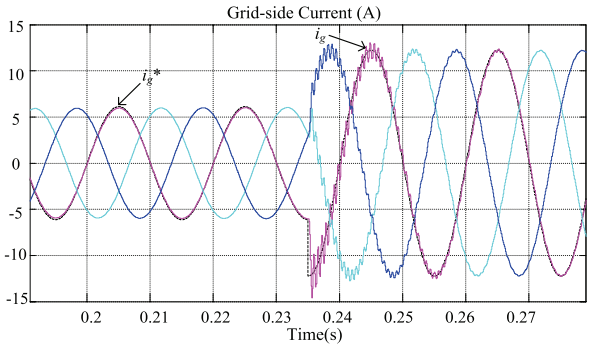

Fig. 16. Grid-side currents waveforms of Case III (low resonant frequency) with active damping

the active damping with capacitor current feedback is used. Applying the parameters described in Table 1 and Table 2, the crossover frequency is set to 1 kHz in order to get a high response and meet the phase margin limitation.

In order to get enough phase margins in Case III, the crossover frequency should be set below the resonant frequency. According to (13), the PR controller gain should be k_p = 0.06. Figure 15 and Fig. 16 show the dynamic performance of Case I and Case III respectively when the reference current changes from 6.5 A to 12.9 A at time 0.235 s to test the dynamic performance. The black dash line is the single phase of the reference grid current $i_g{}^*$. It can be seen from Fig. 15, there is no oscillations during the transient in the high resonant frequency without damping methods. The tracking performance between i_g and $i_g{}^*$ is good.

Figure 16 shows the dynamic performance in the low resonant frequency of the *LLCL* filter when the capacitor current feedback active damping method is used. K_{ic} in Case III is

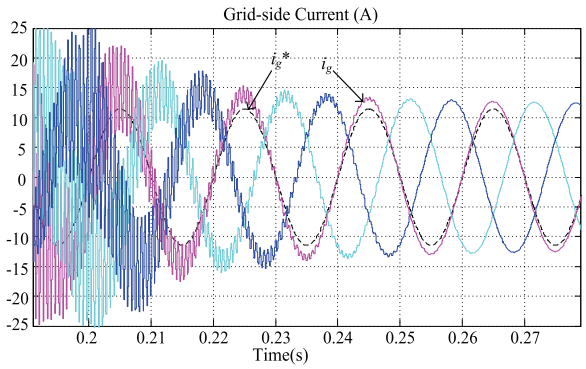

Fig. 17. Grid-side currents waveforms of Case III when active damping is enabled at time 021 s

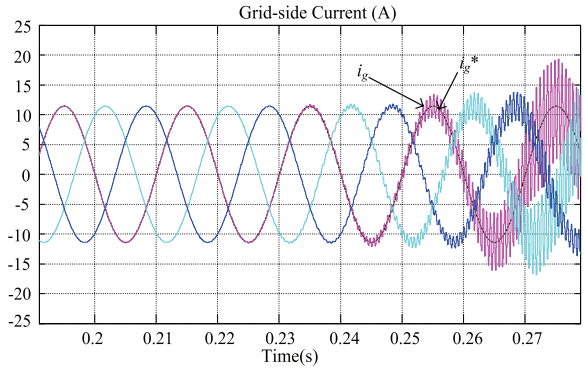

Fig. 18. Grid-side currents waveforms of Case III when K_{ic} is increased at time 0235 s

chosen to be 0.028 according to the design method. It can be seen from Fig. 16 that there is an oscillation when the reference current steps. But it becomes stable after half a period.

Figure 17 shows that the system is unstable at the beginning in the low resonant frequency case, but it turns out to be stable when active damping is enabled at 0.21s in Case III. After three period circles the grid current tracks the reference current. Fig.18 shows that the system becomes unstable when the value of the capacitor feedback coefficient is increased to 0.05. There is a limited stable region for the feedback coefficient, which verifies the analysis in Fig. 7.

5.2 Experimental Results The experimental setup consists of a 2.2 kVA Danfoss three-phase converter connected to the grid through an isolating transformer and the DC-link supplied by Delta Elektronika power sources. The control algorithm is implemented on a dSPACE DS1103 board. Due to the limitation of the setup, the power in the experiment is lower than in the simulation. The system parameters are listed in Table 1 and Table 2.

Figure 19 shows the dynamic transition of the grid-side currents and L_f-C_f circuit voltage in the high resonant frequency case (Case I) when the power is increased without active damping. The reference current steps from 2.4 A–4.8 A and the system can be stable without damping, when the ratio of the resonant frequency to the control frequency is higher than 1/6. Figure 20 shows the grid-side currents and L_f-C_f circuit voltage when the active damping is enabled in the low resonant frequency case (Case III). The capacitor current proportional feedback active damping is used. The system cannot be stable without damping, when the ratio of the resonant

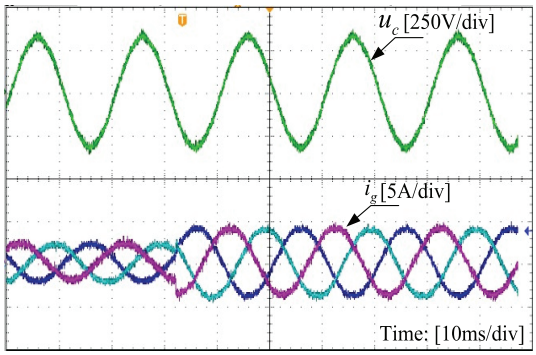

Fig. 19. Experimental results in high resonant frequency case I without active damping

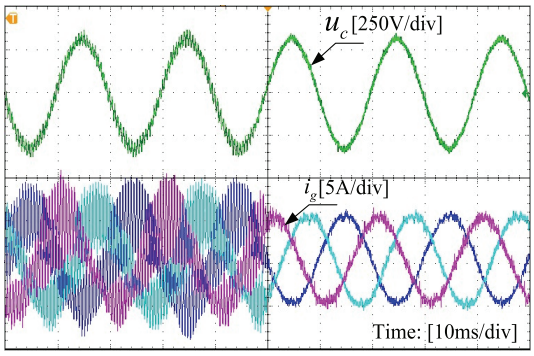

Fig. 20. Experimental results in low resonant frequency case III when active damping is enabled

frequency to the control frequency is lower than 1/6.

6. Conclusion

Compared with the *LCL* filter, the resonant frequency of *LLCL*-filter is higher and it is easier to be stable. The work presented in this paper shows when damping method is not required for an *LLCL* filter considering different sampling and transport delays. The critical frequency is determined by the delay time and sample frequency.

In the low resonant frequency case, or critical case, the resonant frequency is easy to be changed due to the parameter variation and the grid impedance variation. Then, the damping methods are necessary to be used. Based on the analysis of possible feedback variables, the capacitor current feedback active damping control strategy is chosen for the *LLCL* filter. Simulation and experimental results prove the influence of the resonant frequency and the design of capacitor current proportional feedback. The control of the *LCL* filter and *LLCL* filter are similar and the additional inductor of *LLCL* filter brings no extra control difficulties.

References

(1) F. Blaabjerg, R. Teodorescu, M. Liserre, and A. Timbus: "Overview of control and grid synchronization for distributed power generation systems", *IEEE Trans. on Industrial Electronics*, Vol.53, No.5, pp.1398–1409 (2006)

(2) V. Salas and E. Olías: "Overview of the state of technique for PV inverters used in low voltage grid-connected PV systems: Inverters above 10 kW", *Renewable Sustainable Energy Reviews*, Vol.15, No.2, pp.1025–1257 (2011)

(3) W. Wu, Y. He, and F. Blaabjerg: "An LLCL power filter for single-phase grid-tied inverter", *IEEE Trans. Power Electronics*, Vol.27, No.2, pp.782–789 (2012)

(4) J.M. Bloemink and T.C. Green: "Reducing Passive Filter Sizes with Tuned Traps for Distribution Level Power Electronics", in Proc. of IEEE EPE, pp.1–9 (2011)

(5) K. Dai, K. Duan, X. Wang, and Y. Kang: "Application of an LLCL Filter on Three-Phase Three-Wire Shunt Active Power Filter", in Proc. of IEEE INTELEC, pp.1–5 (2012)

(6) A.M. Cantarellas, E. Rakhshani, D. Remon, and P. Rodriguez: "Design of the LCL+trap filter for the two-level VSC installed in a large-scale wave power plant", in Proc. of IEEE Energy Conversion Congress and Exposition (ECCE), pp.707–712 (2013)

(7) J. Dannehl, M. Liserre, and F. Fuchs: "Filter-based active damping of voltage source converters with LCL filters", *IEEE Trans. on Industrial Electronics*, Vol.58, No.8, pp.3623–3633 (2011)

(8) H. Takahashi and J. Itoh: "Damping Control of Filter Resonance Focusing on Output Stage for Multi-Modular Matrix Converter", *IEEJ Trans. EEE*, Vol.2, No.5, pp.242–251 (2013)

(9) C. Bao, X. Ruan, X. Wang, W. Li, D. Pan, and K, Weng: "Design of injected grid current regulator and capacitor-current-feedback active-damping for LCL-type grid-connected inverter", in Proc. of Energy Conversion Congress and Exposition (ECCE), pp.579–586 (2012)

(10) J. Dannehl, F. Fuchs, and S. Hansen: "Investigation of active damping approaches for PI-based current control of grid-connected pulse width modulation converters with LCL filters", *IEEE Trans. on Industry Application*, Vol.46, No.4, pp.1509–1517 (2010)

(11) S. Parker, B. McGrath, and G Holmes: "Regions of Active Damping Control for LCL Filters", in Proc. of IEEE Energy Conversion Congress and Exposition (ECCE), pp.53–60 (2012)

(12) D. Pan, X. Ruan, C. Bao, W. Li, and X. Wang: "Capacitor-Current-Feedback Active Damping With Reduced Computation Delay for Improving Robustness of LCL-Type Grid-Connected Inverter", *IEEE Trans. on Power Electronics*, Vol.29, No.7, pp.3414–3427 (2014)

(13) W. Wu, Y. He, and F. Blaabjerg: "A New Design Method for the Passive Damped LCL- and LLCL-Filter Based Single-Phase Grid-tied Inverter", *IEEE Trans. on Industrial Electronics*, Vol.60, No.10, pp.4339–4350 (2013)

(14) R. Peña-Alzola, M. Liserre, F. Blaabjerg, R. Sebastián, J. Dannehl, and F.W. Fuchs: "Analysis of the Passive Damping Losses in LCL-Filter-Based Grid Converters", *IEEE Trans. on Power Electronics*, Vol.28, No.6, pp.2642–2646 (2013)

(15) P. Channegowda and V. John: "Filter Optimization for Grid Interactive Voltage Source Inverters", *IEEE Trans. on Industrial Electronics*, Vol.57, No.12, pp.4106–4114 (2010)

(16) D.G. Holmes, T.A. Lipo, B.P. McGrath, and W.Y. Kong: "Optimized design of stationary frame three phase AC current regulators", *IEEE Trans. on Power Electronics*, Vol.24, No.11, pp.2417–2425 (2009)

(17) IEEE Recommended Practices and Requirements for Harmonic Control in Electrical Power Systems, IEEE 519-1992 (1992)

(18) M. Huang, W. Wu, Y. Yang, and F. Blaabjerg: "Step by Step Design of a High Order Power Filter for Three-Phase Three-Wire Grid-connected Inverter in Renewable Energy System", in Proc. of PEDG 2013, pp.1–8 (2013)

(19) V. Blasko and V. Kaura: "A novel control to actively damp resonance in input LC filter of a three-phase voltage source converter", *IEEE Trans. on Industry Application*, Vol.33, No.2, pp.542–550 (1997)

(20) S. Yang, Q. Lei, P. F.Z., and Z. Qian: "A Robust Control Scheme for Grid-Connected Voltage-Source Inverters", *IEEE Trans. on Power Electronics*, Vol.58, No.1, pp.202–212 (2011)

(21) X. Wang, P.C. Loh, and F. Blaabjerg: "Design-Oriented Analysis of Resonance Damping and Harmonic Compensation for LCL-Filtered Voltage Source Converters", in *Proc. of ECCE*, pp.1194–1201 (2014)

(22) C. Liu, X. Zhang, L. Tan, and F. Liu: "A novel control strategy of LCL-VSC based on notch concept", in Proc. of PEDG, pp.343–346 (2010)

(23) M. Huang, X. Wang, P.C. Loh, and F. Blaabjerg: "Resonant-inductor-voltage feedback active damping based control for grid-connected inverters with LLCL-filters", in Proc. of ECCE, pp.1194–1201 (2014)

(24) Y. Tang, P.C. Loh, P. Wang, F.H. Choo, and F. Gao: "Exploring inherent damping characteristics of LCL-filters for three-phase grid connected voltage source inverters", *IEEE Trans. on Power Electronics*, Vol.27, No.3, pp.1433–1443 (2012)

(25) L. Kuo and S. Mat: "Steady-state solutions of a voltage source converter with dq-frame controllers by means of the time-domain method", *IEEJ Trans. EEE*, Vol.9, No.2, pp.165–175 (2014)

(26) M. Xue, Y. Zhang, Y. Kang, Y. Yi, S. Li, and F. Liu: "Full feed forward of grid voltage for discrete state feedback controlled grid-connected inverter with LCL filter", *IEEE Trans. on Power Electronics*, Vol.27, No.10, pp.4234–4247 (2012)

Min Huang (Non-member) received the B.S. degree in Electrical Engineering from Anhui University of Technology, Anhui, China, in 2010, and the M.Sc. degree in Electrical Engineering from Shanghai Maritime University, Shanghai, China, in 2012. She is currently working toward the Ph.D. degree in the Institute of Energy Technology, Aalborg University, Aalborg, Denmark. Her research interests include power quality, control and power converters for renewable energy systems.

Xiongfei Wang (Non-member) received the B.S. degree from Yanshan University, Qinhuangdao, China, in 2006, the M.S. degree from Harbin Institute of Technology, Harbin, China, in 2008, both in electrical engineering, and the Ph.D. degree from Aalborg University, Aalborg, Denmark, in 2013. Since 2009, he has been with the Aalborg University, Aalborg, Denmark, where he is currently an Assistant Professor in the Department of Energy Technology. His research interests include modeling and control of power converters, grid converters for renewable energy systems and microgrids, harmonic analysis and stability of power electronics based power systems. Dr. Wang is an Associate Editor of IEEE TRANSACTIONS ON INDUSTRY APPLICATIONS. He serves as a Guest Associate Editor of IEEE JOURNAL OF EMERGING AND SELECTED TOPICS IN POWER ELECTRONICS Special Issue on Harmonic Stability and Mitigation in Power Electronics Based Power Systems.

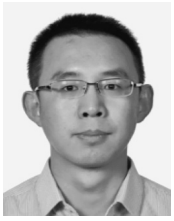

Poh Chiang Loh (Non-member) received the B. Eng. (Hons.) and M.Eng degrees from the National University of Singapore, Singapore, in 1998 and 2000, respectively, and the Ph.D. degree from Monash University, Melbourne, Australia, in 2002, all in electrical engineering. During the summer of 2001, he was a Visiting Scholar with the Wisconsin Electric Machine and Power Electronics Consortium, University of Wisconsin-Madison, where he was involved in the synchronized implementation of cascaded multilevel inverters, and reduced common mode carrier-based and hysteresis control strategies for multilevel inverters. From 2002 to 2003, he was a Project Engineer with the Defense Science and Technology Agency, Singapore, managing major defense infrastructure projects and exploring new technology for defense applications. From 2003 to 2009, he was an Assistant Professor and then an Associate Professor with the Nanyang Technological University, Singapore. In 2005, he was a Visiting Staff member first at the University of Hong Kong, and then at Aalborg University, Denmark. In 2007 and 2009, he again returned to Aalborg University first as a Visiting Staff member working on matrix converters and the control of grid-interfaced inverters, and then as a Guest Member of the Vestas Power Program.

Frede Blaabjerg (Non-member) was with ABB-Scandia, Randers, Denmark, from 1987 to 1988. From 1988 to 1992, he was a Ph.D. Student with Aalborg University, Aalborg, Denmark. He became an Assistant Professor in 1992, an Associate Professor in 1996, and a Full Professor of power electronics and drives in 1998. His current research interests include power electronics and its applications such as in wind turbines, PV systems, reliability, harmonics and adjustable speed drives. He has received 15 IEEE Prize Paper Awards, the IEEE PELS Distinguished Service Award in 2009, the EPE-PEMC Council Award in 2010, the IEEE William E. Newell Power Electronics Award 2014 and the Villum Kann Rasmussen Research Award 2014. He was an Editor-in-Chief of the IEEE TRANSACTIONS ON POWER ELECTRONICS from 2006 to 2012. He has been Distinguished Lecturer for the IEEE Power Electronics Society from 2005 to 2007 and for the IEEE Industry Applications Society from 2010 to 2011. He is nominated in 2014 by Thomson Reuters to be between the most 250 cited researchers in Engineering in the world.

Weimin Wu (Non-member) received Ph.D. degrees from the College of Electrical Engineering, Zhejiang University, Hangzhou, China, in 2005. He worked as a research engineer in the Delta Power Electronic Center (DPEC), Shanghai, from July, 2005 to June, 2006. Since July, 2006, he has been a Faculty Member at Shanghai Maritime University, where he is currently a full Professor in Department of Electrical Engineering. He was a Visiting Professor in the Center for Power Electronics Systems (CPES), Virginia Polytechnic Institute and State University, Blacksburg, from Sept. 2008 to March. 2009. From Nov. 2011 to Jan. 2014, he was also a visiting professor in the Department of Energy Technology, working at the Center of Reliable Power Electronics (CORPE). He has coauthored over 60 papers and holds five patents. His areas of interests include power converters for renewable energy systems, power quality, smart grid, and energy storage technology.